Electric Power Systems Research 214 (2023) 108914

Contents lists available at ScienceDirect

Electric Power Systems Research

journal homepage: www.elsevier.com/locate/epsr

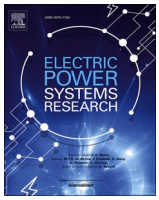

Multi-objective optimal allocation of distributed generation considering the spatiotemporal correlation of wind-photovoltaic-load

Fengyang Gao [a], Cheng Yuan [b,*], Zhaojun Li [a], Shengxian Zhuang [c]

[a] School of Automation and Electrical Engineering, Lanzhou Jiaotong University, Lanzhou 730070, China
[b] Beijing Tsintergy Technology Co., Ltd., Beijing 100084, China
[c] School of Electrical Engineering, Southwest Jiaotong University, Chengdu 610031, China

ARTICLE INFO

Keywords:
Spatiotemporal correlation
Distributed generation
Scenario generation
Multi-objective optimal allocation
Bayesian network structural learning

ABSTRACT

Aiming at the problem of the distributed generation (DG) planning caused by the strong spatiotemporal coupling between DG output and load demand in adjacent areas, a multi-objective planning model is proposed to describe the spatiotemporal correlation of sources. By combining the most weight supported tree (MWST) and depth first search (DFS), the method achieves the a priori requirement for constructing bayesian network (BN) structure using the K2 algorithm. Then, the MDK2-BN model is established through the measured data, which can describe the correlation between multi-dimensional wind-photovoltaic-load. A DG multi-objective programming model with maximum annual profit rate and minimum comprehensive operation risk is constructed. The results has three main advantages: (1) the MDK2-BN structure can achieve satisfactory results when dealing with small networks. (2) the MDK2-BN model conforms to the spatiotemporal correlation of the DG output, and the proposed configuration can improve the access capacity of DG. (3) the favorable level of the DG's grid connection can be effectively improved by considering the seasonal difference in performance and providing the planners with the decision-making references that balance the economic benefits, system operational safety, and environmental benefits.

1. Introduction

1.1. Motivation

DG has developed from marginal to a mainstream factor in the power grid [1,2]. However, intermittent DG has characteristics of randomness and correlation, which bring considerable challenges to the planning and operation of power grids. The optimal DG configuration depends on the economics of investment and operation, and the risks associated with the system operation [3–5]. Due to a strong spatiotemporal coupling of DG output and load in neighboring regions with similar environmental and meteorological conditions [6,7], it is necessary to develop a wind-photovoltaic-load output model and a reasonable planning model to achieve economic, operation safety, and environmental benefits of operating power grid in the market environment.

The nonlinear correlation between the DG output and load demand in adjacent areas is difficult to uniformly describe. The BN model that consider the coupling of variables in multi-dimensional data can be used to extract the correlation features and construct multivariate forecasting models [8,9]. In one of the recent studies [10], a BN model describing the correlation between wind speed, light intensity, and load, is established and its effectiveness is verified. In another study [11], a BN conforming to the actual operating state of the wind turbine is established using the multi-dimensional data to determine the correlation between multiple parameters and evaluate the machine capacity reduction at high temperatures.

Although the aforementioned studies have proposed effective and accurate models, there have still been some constraints in BN model. First, the strength of the correlation between the chosen variables, but this is related to the strong correlation between the DG output and load demand in neighboring regions. The second constraint is how to determine the optimal BN structure using the data [12–15].

1.2. Literature review

In order to address the planning issues of DG in the power grid, In Ref. [16,17], the negative correlation between the wind speed and load is considered and focused on the effects of correlation on generator

* Corresponding author.
E-mail address: cheng_y1108@163.com (C. Yuan).

https://doi.org/10.1016/j.epsr.2022.108914
Received 4 March 2021; Received in revised form 17 October 2022; Accepted 18 October 2022
Available online 29 October 2022

planning. In Ref. [18], the effects of active management is considered when a large-scale photovoltaic is connected to the grid, and a multi-objective model with the largest energy penetration rate and the smallest voltage deviation is established. In Ref. [19], the temporal correlation between the wind speed and load is studied and a site location and capacity model for wind power generators is established. In the mentioned studies, different mathematical models for multi-objective DG planning have been established from the perspectives of investment interest, power grid operation safety, and environmental factors. However, these models treat the DG connection explicitly, which makes them be too narrowly focused and disable them to satisfy the freedom of choice for the supply side and customers introduced by the reform of the power system. In order to construct a comprehensive spatiotemporally correlated wind–photovoltaic–load model to solve the problem of DG grid connection planning, In Ref. [20], joint probability distribution method and scenario-reduction technique are used to target the maximum DG capacity grid connection and a multi-scenario model by introducing active management constraints is built. However, this model considers only the grid connection by a single wind power generator or a single photovoltaic connection, which is not applicable to the planning of a large-scale DG grid-connection. In other studies [21–23], the effect of temporal fluctuation of the DG output on the grid configuration is analyzed using a clustered multi-scenario probability analysis method; however, the computation complexity of a multi-scenario situation is high, and the roughness of the generic clustering method adversely affects the overall optimization decision. The fitting degree between different variables can be assessed reasonably by the score-and-search method represented by the K2 algorithm.

1.3. Contribution

In this paper, a multi-objective DG planning model based on the MDK2-BN model is developed from the perspective of multi-dimensional data mining. First, the MWST and DFS are combined to satisfy the *a priori* requirement for constructing the BN structure using the K2 algorithm, and then, an MD-K2 BN structure is defined. Next, the correlation analysis is conducted considering the BN requirements for wind speed, light intensity, and load demand of adjacent regions in order to achieve a more accurate generation of multiple scenarios. The scenarios are further compressed using a highly efficient H-K composite clustering algorithm [23]. By considering the spatiotemporal correlation of the source terminal and the indicators of the economy, system safety, and environmental benefit, a multi-objective DG planning model is constructed with the main objectives of maximum annual profit rate and minimum comprehensive operation risk. The constructed model is solved by an improved multi-objective particle swarm optimization (IMPSO) algorithm, and a nonlinear adjustment method is proposed to dynamically change the inertia weight and improve the global optimization ability. Finally, the model validity is verified by a simulation on IEEE 33-bus test systems.

In specific, this work contributes to the literature in:

- A method to solve the correlation analysis for wind speed, light intensity, and load demand of adjacent regions in order to achieve a more accurate generation of multiple scenarios.
- A multi-objective DG planning model of considering the spatiotemporal correlation, economic and system safety and environmental benefits.
- The effects of the seasonal difference on the favorable level of the DG's grid connection have been investigated.

Section II presents the probability model of distributed generation output, including wind turbine generators and photovoltaic generators. Section III describes MDK2-BN model as well as multi-scenario generation with the spatiotemporal correlation of wind-photovoltaic-load using the methodology. Section IV presents the multi-objective planning model, and Section V describes an IMPSO algorithm. Section VI generalizes reports the results and the conclusion is generalized in section VII.

2. Probability model of distributed generation output

The active output power of wind turbine is mainly affected by wind speed. The prerequisite for analyzing the impact of wind power grid connection is to accurately describe the wind speed-power characteristic curve for wind turbine.

2.1. Probabilistic model of wind turbine generators output

The wind speed of wind turbine generators (WTG) is the main factor affecting the output active power. The wind speed-power characteristic curve is the basis of WTG planning and an important indicator for evaluating the performance and generation capacity. Assuming thatv_r,v_i and$v_o$are rated wind speed, cut-in wind speed, cut-out wind speed, respectively, the relationship between WTG output power (P_{WTG}) and rated output power (P^r_{WTG}) is established by parameter method as follows [24]:

$$P_{WTG}=\begin{cases}0\ , & v\le v_i \text{ or } v>v_o\\ P^r_{WTG}\dfrac{v-v_i}{v_r-v_i}, & v_i<v\le v_r\\ P^r_{WTG}\ , & v_r<v\le v\end{cases} \tag{1}$$

Reactive power of WTG can be expressed as the relationship between power factor angle (φ_{WTG}) and P_{WTG} as follows:

$$Q_{WTG}=P_{WTG}\tan\varphi_{WTG} \tag{2}$$

2.2. Probabilistic model of photovoltaic generators output

The output of a photovoltaic generators (PVG) is subject to many factors. The current research usually uses light intensity (E) to approximate the output of PVG, and establishes the relationship between PVG output power (P_{PVG}), rated output power (P^r_{PVG}) and rated light intensity (E^r) by parameter method as follows:

$$P_{PVG}=\begin{cases}P^r_{PVG}\dfrac{E}{E^r} & E\le E^r\\ P^r_{PVG} & E>E^r\end{cases} \tag{3}$$

Reactive power of PVG can be expressed as the relationship between power factor angle (φ_{PVG}) and P_{PVG} as follows:

$$Q_{PVG}=P_{PVG}\tan\varphi_{PVG} \tag{4}$$

3. Scene generation of wind-photovoltaic-load based on MDK2-BN model

3.1. Basic theory of BN

With the development of big data as a research field, the research on solving the uncertainty problems considering the combination of probability theory and graph theory has become a hot research topic. The BN represents a probabilistic graphical model for modeling complex systems with variables of different properties, which is capable of describing the uncertainty of variables and correlation between them. A complete BN includes the following two parts:

(1) The network structure represents a directed acyclic graph (DAG) with n nodes (X_1, X_2, …, X_n). Through the directed edges of the structure, the DAG can describe the relationships between the nodes.
(2) The conditional probability associated with all the nodes is expressed as a set $p(X_i|\prod(X_i))$, where $\prod(X_i)$ represents the direct

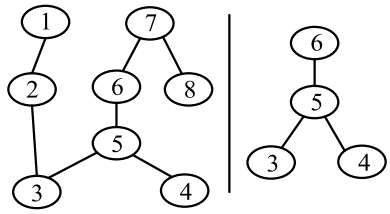

Fig. 1. Most weight supported tree and the most node connection.

parent nodes of X_i. By applying the chain rule, the joint probability distribution can be obtained as follows:

$$p(X_1, X_2, \cdots, X_n) = \prod_{k=1}^{n} p\left(X_i \middle| \prod(X_i)\right) \tag{5}$$

The investigation of BN mainly consists of structural learning and parametric learning [25–27]. For a given network structure, it is easy to acquire the relevant parameters from a large amount of data, but different characters of the input data pose a challenge to the network structure prediction. Thus, in the BN construction, the crucial thing is to construct a BN structure that represents relationships between input parameters accurately.

3.2. Generation of MDK2-BN

The K2 algorithm has often been used in the construction of a DAG structure [28]. In order to satisfy the *a priori* requirement that the K2 algorithm depends on the maximum number of parent nodes and the order of nodes, the node order is optimized by the joint use of the MWST and the DFS and by analyzing the attribute relationship of two variables in the topological sequence. The MWST defines the dependence between variables through mutual signals. Namely, the magnitude of the mutual signal represents the strength of the correlation between variables. The mutual signal is calculated using the self-probabilities $P(X_i)$ and $P(X_j)$ of nodes i and j and their joint probability $P(X_i, X_j)$:

$$I(X_i; X_j) = \sum_{X_i X_j} P(X_i, X_j) \log \frac{P(X_i, X_j)}{P(X_i) P(X_j)} \tag{6}$$

When $I(X_i; X_j) > 0$, nodes i and j have a dependence relationship. The dependence degree of variables is represented by nodes connected to undirected sides by traversing all the mutual signal values. The connection relationship between the MWST and the maximum nodes is presented in Fig. 1.

Compared to a randomly searched node sequence, a topological sequence based on the DFS can effectively reduce the search space [29]. When the correct node sequence is maintained, the K2 algorithm can lead to an optimized network structure combined with DFS. For a given connection map, the basic steps of the DFS are as follows:

Step 1: Access a vertex v and scan adjacent points of v; next, successively perform the DFS with a search strategy to increase the vertical depth of the search map.

Step 2: Begin to backtrack in the search and check whether there are other unvisited critical points on the previous path, and repeat step 1.

Step 3: Repeat the Step 1—2 until all vertices are visited.

In the route search process, the computation volume increases with the complexity degree of the map. For a flow map with n vertices, after entering the stack at vertex v, the time complexity to establish a chain stack is O(n). Next, the connection table of each node is scanned, having a complexity level of O(e) and the number of sides m in the undirected map ($e = e_1 + e_2 + \ldots + e_k$). The total time complexity is O(n+e), and good results can be obtained without shrinking the search space when dealing with small networks. The DAG of the Bayesian network is determined by comparing the score value using the K2 algorithm.

After determining the DAG of BN, the parameters of each node need to be determined, that is, a conditional probability table representing the degree of influence between various variables is established. This paper uses the maximum likelihood estimation (MLE) to calculate the conditional probability table of each node [30]. Assuming that the historical data set is $U = \{U_1, U_2, \cdots, U_m\}$, and because the node variables in BN are usually discrete variables. First, the characteristic function is defined as follows:

$$H_{i,j,m,k} = \begin{cases} 1, & [X_m = k, \pi(X_i) = j] \\ 0, & \text{others} \end{cases} \tag{7}$$

Therefore, the likelihood function is as follows:

$$\begin{aligned} L &= \sum_i \sum_m \log \prod_{j,k} \theta_{i,j,m,k} H_{i,j,m,k} = \sum_i \sum_m \sum_{j,k} H_{i,j,m,k} \log \theta_{i,j,m,k} \\ &= \sum_{i,j,k} \sum_m H[X_n = k, \pi(X_i) = j] \log \theta_{i,j,m,k} \end{aligned} \tag{8}$$

here, i is the node variable;$\theta_{i,j,m,k} = P(X_n = k | \pi(X_i) = j)$ represents the state parameter when the parent node takes j and the child node is equal to k, and$\theta_{i,j,m,k} = P(X_n = k | \pi(X_i) = j)$; and $H[X_n = k, \pi(X_i) = j]$ records the number of occurrences of historical data $[X_m = k, \pi(X_i) = j]$.

Finally, the MLE of $\theta_{i,j,m,k}$ can be calculated by lagrange multiplier method as follows:

$$\theta_{i,j,m,k} = \frac{\sum_m H[X_n = k | \pi(X_i) = j]}{\sum_i \sum_m H[X_n = k | \pi(X_i) = j]} \tag{9}$$

3.3. Multi-scenario generation with the spatiotemporal correlation of wind-photovoltaic-load

This paper uses historical data to describe the randomness and spatiotemporal correlation of wind-photovoltaic-load. Assuming that there are already M groups of known data on wind speed, light intensity and load, the steps to generate spatiotemporal correlation samples are as follows:

(1) Due to equipment malfunctions, data transmission limitations, and other reasons, the original dataset can miss certain data parts. Therefore, in order to preprocess the data, the data is processed by the mean interpolation method, and anomalous data points are deleted.
(2) The edge distribution functions of the wind speed, light intensity and load, denoted as a set $Y = [y_1, y_2, \cdots, y_m]$, are estimated by the kernel density estimation method. The Bayesian network modeling realizes the discretization of continuous data values. Datasets with continuous characteristics are processed by the classic data mining K-mean clustering algorithm to achieve data segmentation.
(3) The MWST is established according to the sample data, and dependencies between variables are determined based on the mutual signal so as to calculate the maximum number of parent nodes μ. The node topology sequence ρ is obtained by the DFS. The K2 algorithm is used to obtain the DAG of the BN, and the BN model is completed using the relevant parameters calculated according to the MLE.
(4) Then, the network model is sampled, and the initial scenario of the wind–photovoltaic–load with the spatiotemporal correlation is generated by an inverse transformation $Y^{-1}(\cdot)$ of the edge distribution function. Finally, the number of scenarios is reduced by the HK compound clustering algorithm, and the wind–photovoltaic–load planning scenario is obtained from the probability model of distributed generation output.

4. Multi-objective planning model

4.1. Objective function

In order to satisfy the economic operation of distribution network and reduce the operational risk considering source-load uncertainty, and the objective functions of the multi-objective DG planning include maximizing the average annual profit rate of DG and minimizing the system risk.

4.1.1. The average annual profit rate of DG

The average annual profit rate of DG is numerically equal to the ratio of the average annual income of DG (I_P) to the average annual investment cost (C_Y).

$$\max f_1 = \frac{I_P}{C_Y} \tag{10}$$

the calculation formula of C_Y as follows:

$$\begin{cases} C_Y = C_I + C_{OM} + C_{IL} + C_P \\ C_I = \dfrac{y_0(1+y_0)^{n_{WG}}}{(1+y_0)^{n_{WG}}-1}\sum\limits_{i=1}^{N}\left(c^I_{WG}P^r_{WGi}\right) \\ \quad + \dfrac{y_0(1+y_0)^{n_{PG}}}{(1+y_0)^{n_{PG}}-1}\sum\limits_{i=1}^{N}\left(c^I_{PG}P^r_{PGi}\right) \\ C_{OM} = \sum\limits_{i=1}^{N}\left(c^{OM}_{WG}E_{WGi} + c^{OM}_{PG}E_{PGi}\right) \\ C_{IL} = c_{IL}\sum\limits_{i=1}^{N}P_{ILi} \\ C_P = c_P E_g \end{cases} \tag{11}$$

here,$C_I$represents the investment cost of DG converted to each year; C_{OM}means operation and management cost of DG; C_{IL}represents annual compensation of interrupted load; $C_P$determines the cost of power supplement from substation; $c^I_{WG}$and$c^I_{PG}$are the per-unit investment cost of WTG and PVG; $P^r_{WGi}$and$P^r_{PGi}$are the installed capacity of WTG and PVG at bus i; $y_0$is the discount rate; $n_{WG}$and$n_{PG}$are the economic life of WTG and PVG; N is the number of grid buses;$c^{OM}_{WG}$and$c^{OM}_{PG}$are the per-unit operation and management cost of WTG and PVG; $E_{WGi}$and$E_{PGi}$are the annual power generation of WTG and PVG; c_{IL}determines the per-unit compensation of interrupted load; $P_{ILi}$is the annual interruption of interrupted load at bus i. the calculation formula of$I_P$as follows:

$$\begin{cases} I_P = I_S + I_G + I_R + I_E \\ I_E = V_{e1} + V_{e2} + V_{e3} \end{cases} \tag{12}$$

here, I_S and I_G describe the annual income of net electricity and price subsidy of DG; $I_R$is the annual income sold to users; $I_E$is the environmental benefits of DG energy conservation and emission reduction, specifically, and $I_E$can be equivalent to the sum of the value of fuel consumed by traditional power plants (V_{e1}), the environmental value of gas pollutants (V_{e2}) and heavy metal emission reduction (V_{e3}).

4.1.2. The comprehensive operation risk of the system

Since DG planning is based on forecast data of wind-photovoltaic-load, its strong uncertainty characteristics increase the over-limit probability of the state variables of the distribution network. Considering the correlation between the system bus and branch, the state variables tend to change in the same direction. Therefore, comprehensively considering the risk of voltage over-limit of all buses and the power flow over-limit of all branches [31], the comprehensive operational risk index of the system is defined as follows:

$$\min f_2 = \alpha_1 P_u + \alpha_2 P_l \tag{13}$$

here,$P_u$and$P_l$are the risk index of voltage over-limit and the power flow over-limit; $\alpha_1$and$\alpha_2$represent comprehensive operating weight coefficient, $\alpha_1 + \alpha_2 = 1$.

Because the calculation method of$P_u$andP_l are similar, the following uses P_u as an example to give the relevant calculation method, and the calculation process of B will not be repeated.

$$P_u = \left[\frac{\beta_1}{N}\sum_s\sum_i\left|S\left(U_{s,i,t}\right)\right| + \beta_2 \max_{s,i}\left|S\left(U_{s,i,t}\right)\right|\right] \tag{14}$$

here, the first term and the second term represent the average and maximum value of the risk index of voltage over-limit of all buses respectively; $\beta_1$and$\beta_2$are the weight coefficient of voltage risk, $\beta_1 + \beta_2 = 1$, and the different values of$\beta_1$and$\beta_2$can increase or decrease the influence of the average value and the maximum value, to eliminate the shadowing of indicators to the greatest extent; $U_{s,i,t}$is the bus voltage at bus i for the sth scene,$S(\cdot)$describes the loss severity of voltage over-limit. and,

$$\begin{cases} S\left(U_{s,i,t}\right) = e^{\lambda\xi\left(U_{s,i,t}\right)} - 1 \\ \xi\left(U_{s,i,t}\right) = \begin{cases} \left(\dfrac{U_{i,min} - U_{s,i,t}}{U_{i,max} - U_{i,min}}\right)^2, U_{s,i,t} < U_{i,min} \\ 0, \qquad U_{i,min} \le U_{s,i,t} \le U_{i,max} \\ \left(\dfrac{U_{s,i,t} - U_{i,max}}{U_{i,max} - U_{i,min}}\right)^2, U_{s,i,t} > U_{i,max} \end{cases} \end{cases} \tag{15}$$

Here, $\xi(\cdot)$ is the voltage loss; $U_{i,\min}$and$U_{i,\max}$are the allowed lower and upper nodal voltage at bus i; λ is the penalty coefficient of voltage loss, which is used to reflect the degree of nonlinear relationship between $S(\cdot)$ and $\xi(\cdot)$.

4.2. Constraints

4.2.1. Power flow equations

$$\begin{cases} P_{Gi} - P_{Li} - U_i\sum\limits_{i=1}^{N}U_j\left(G_{ij}\cos\theta_{ij} + B_{ij}\sin\theta_{ij}\right) = 0 \\ Q_{Gi} - Q_{Li} - U_i\sum\limits_{i=1}^{N}U_j\left(G_{ij}\sin\theta_{ij} - B_{ij}\cos\theta_{ij}\right) = 0 \end{cases} \tag{16}$$

here, $P_{Gi}$and$Q_{Gi}$are the injection active power and reactive power of DG at bus i; $P_{Li}$and$Q_{Li}$are the injection active power and reactive power of load; $U_i$and$U_j$are the nodal voltage at bus i and bus j; G_{ij} and B_{ij} are the corresponding real and imaginary part of the admittance matrix, respectively; θ_{ij} is the angle difference between bus i and bus j.

4.2.2. Security constraints of the power grid

$$\begin{cases} U_{i,\min} \le U_i \le U_{i,\max} \\ |I_{ij}| \le I_{\max} \\ |P_{ij}| \le P_{\max} \end{cases} \tag{17}$$

here, $I_{\max}$is the allowed upper of branch currentI_{ij};$P_{\max}$is the allowed upper of branch power P_{ij}.

4.2.3. Output constraints of adjustable and controllable resources

$$\begin{cases} 0 \le P^r_{WGi} \le P^{\max}_{WGi} \\ 0 \le P^r_{PGi} \le P^{\max}_{PGi} \\ 0 \le P^r_{WGi} + P^r_{PGi} \le P^{\max}_{DGi} \end{cases} \tag{18}$$

$$\begin{cases} Q_{WGi} = P^r_{WGi}\tan(\varphi_{WGi}) \\ Q_{PGi} = P^r_{PGi}\tan(\varphi_{PGi}) \end{cases} \tag{19}$$

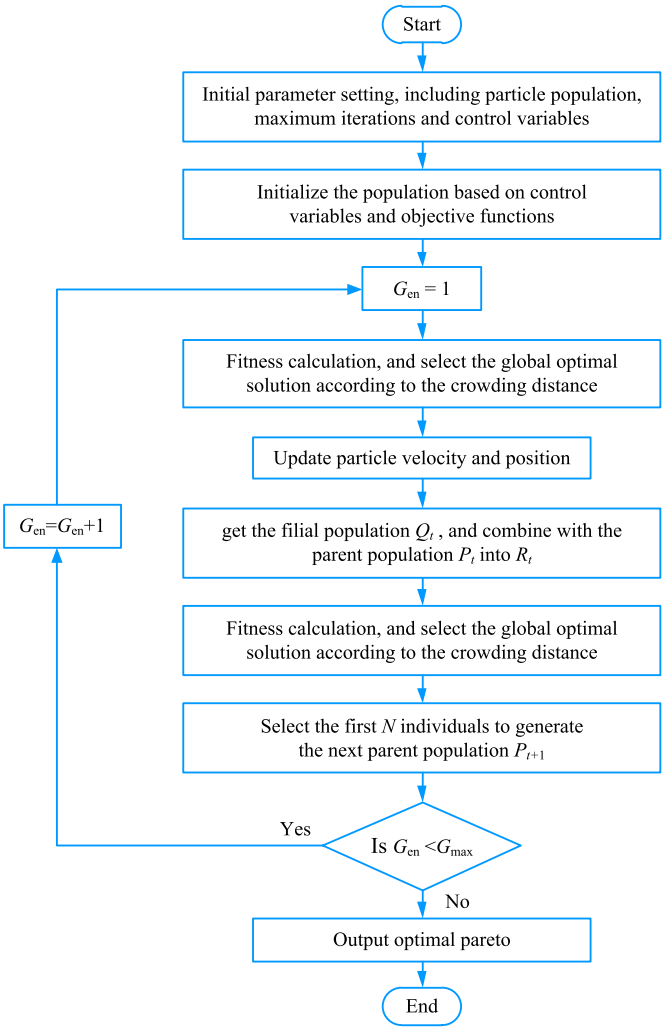

Fig. 2. Process of IMPSO algorithm.

$$0 \le P_{\mathrm{IL}i} \le P_{\mathrm{IL}i}^{\max} \tag{20}$$

here, $P_{\mathrm{WG}i}^{\max}$,$P_{\mathrm{PG}i}^{\max}$and$P_{\mathrm{DG}i}^{\max}$are the maximum allowed installation capacity of WTG, PVG and DG at bus i; $P_{\mathrm{IL}i}^{\max}$is the allowed upper of interrupted load.

5. IMPSO concept and methodology

IMPSO is an intelligent optimization algorithm based on evolutionary group, whose main principle is to keep the particle velocity and position of the search space to find the optimal solution [32–34]. Therefore, IMPSO has a good feature matching with the multi-objective programming problem, and its velocity and position update equations are as follows:

$$v_{id}^{(t+1)} = \omega_i v_{id}^{(t)} + c_1 r_1 \left[p_{idbest}^{(t)} - x_{id}^{(t)}\right] + c_2 r_2 \left[g_{dbest}^{(t)} - x_{id}^{(t)}\right] \tag{21}$$

$$x_{id}^{(t+1)} = x_{id}^{(t)} + v_{id}^{(t+1)} \tag{22}$$

here, $v_{id}^{(t)}$ and $x_{id}^{(t)}$ are the velocity and position of particle i at dth dimension in the tth iteration, respectively; $p_{idbest}^{(t)}$ is the individual optimal position of particle i at dth dimension in the tth iteration; $g_{dbest}^{(t)}$ is the global optimal position in the tth iteration; $c_1$andc_2 are the acceleration coefficient; r_1,r_2~$U(0,1)$; ω_i is the inertia weight.

However, under the guidance of inertial weights or linearly decreasing weights, IMPSO tends to lose population diversity and fall into the trap of local optimality. In order to improve the efficiency of algorithm search, nonlinear adjustment is used to make ω_i dynamically change according to the global optimal position and current position. The improved MOPSO updates the inertia weight as follows:

$$\omega_i = \omega_{\max} - (\omega_{\max} - \omega_{\min})\left(D_i^{(t)} - 1\right)^2 \tag{23}$$

$$D_i^{(t)} = \frac{1}{SN_d}\sum_{d=1}^{N}\left|x_{id}^{(t)} - g_{dbest}^{(t)}\right| \tag{24}$$

here, $D_i^{(t)}$is the difference between the current position and the global optimal position of particle i in the tth iteration; S is the allowed lower and upper of particle i; N_{d} is the spatial dimension; $\omega_{\min}$ and $\omega_{\max}$ are the initial and final values of ω_i, respectively.

In the calculation process, the cumulative rank fitness assignment strategy, the enhanced elite retention strategy and the crowding distance calculation strategy are introduced [35]. The enhancement of the elite retention strategy means that the elite individuals also participate in the renewal. If the fitness decreases after the renewal, the individuals before the renewal are retained, otherwise the renewed individuals participate in the evolution of the next generation. It can effectively improve the convergence ability of the algorithm while preventing premature population. The IMPSO algorithm process is shown in Fig. 2.

In addition, the Pareto optimal solution is selected according to a fuzzy logic decision method, and the preference of the decision-maker is used to measure a near-optimal Pareto solution. For multiple objective sets, the membership degree ζ_s and the linear membership function $\tau_k(f_k^s)$ are defined as follows:

$$\begin{cases} \zeta_s = \sum_k \varpi_k \tau_k\left(f_k^s\right) \\ \tau_k\left(f_k^s\right) = \begin{cases} 1, & f_k^s < f_k^D \\ \dfrac{f_k^U - f_k^s}{f_k^U - f_k^D}, & f_k^D \le f_k^s \le f_k^U \\ 0, & f_k^s > f_k^D \end{cases} \end{cases} \tag{25}$$

where f_k^s is the i-th objective value of the s-Pareto solution; $\varpi_k$is the weight coefficient of the target, which satisfies $\sum_k \varpi_k = 1$; f_k^D and f_k^U are the upper and lower bounds of the kth target, respectively.

6. Numerical results and analysis

6.1. MDK2-BN structure accuracy verification

6.1.1. The performance indexes of MDK2-BN structure

The performance indexes include Bayesian information criterion (BIC) score and accuracy of DAG.

BIC score function is used to evaluate the fitting degree of network structure. According to the decomposability of BIC scoring function, when the local structure in BN changes, in order to reduce the number of repeated calculations, only use Eq. (25) to calculate the score $B_{\mathrm{new}}(\boldsymbol{G}_1,D)$ of the changed local structure $\boldsymbol{G}_1$, and then substitute Eq. (26) to get the overall score $B(\boldsymbol{G},D)$.

$$\begin{aligned} B_{\mathrm{new}}(\mathbf{G}_1, D) &= \sum_{i\in G_1} B(X_i, \pi(X_i)) \\ &= \sum_{i\in G_1}\left(\sum_{j=1}^{q_i}\sum_{k=1}^{r_i}\theta_{i,j,m,k}\log\frac{\theta_{i,j,m,k}}{\sum_{k=1}^{r_i}\theta_{i,j,m,k}} - \frac{q_i(r_i-1)}{2}\log m\right) \end{aligned} \tag{26}$$

$$B(\mathbf{G}, D) = B_{\mathrm{new}}(\mathbf{G}_1, D) + B_{\mathrm{old}}(\mathbf{G}_2, D) \tag{27}$$

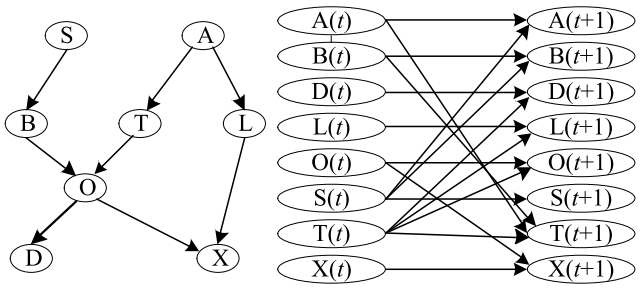

Fig. 3. Standard ASIA network and transfer relations.

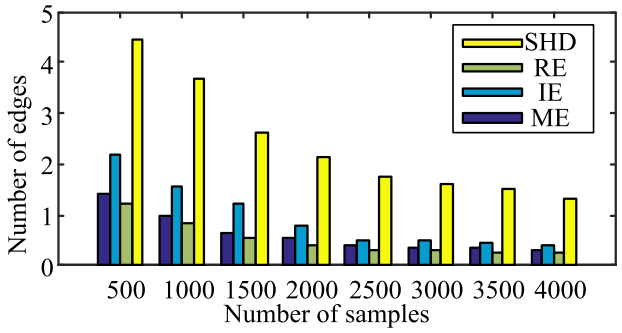

Fig. 4. DAG evaluation index results.

where q_i indicates that the value of $\pi(X_i)$ has a total of q_i combinations; r_i means X_i has a total of r_i values; m is the number of models.

The performance indexes of DAG include:

- Increasable edge (IE), represents the edge that the prediction structure is independent of the standard structure.
- Missing edge (ME), represents the missing edge of the prediction structure compared with the standard structure.
- Reversed edge (RE), represents the opposite edge of the predicted structure compared to the standard structure.

6.1.2. *Numerical results of MDK2-BN structure accuracy*

The operating environment is MATLAB 2016a, and the hardware configuration is a computer with CPU Intel Core i5-4210M 3.60GHz.

In order to verify the Bayesian network DAG learning capability described in Section 3.2, structural learning is conducted on the standard Asia network. The small network has eight nodes and eight edges, and the corresponding *a priori* network and transformation relationship are shown in Fig. 3. Eight training sample datasets of different sizes are randomly generated. In order to reduce the effect of random data on the experiment, each training set is generated ten times and run ten times individually. The calculated average of 100 runs is used as the final result of the experiment.

The results of the DAG evaluation index are shown in Fig. 4. The variation of the IE shows that the number of reverse edges gradually approached to zero as the number of datasets increased; thus, the topological sequence obtained by the joint MWST and the node sequence obtained by the DFS are almost the same, so the number of reverse edges could be reduced after substituting into the K2 algorithm. Both the ME and RE indicators demonstrated the accuracy of the MDK2-BN structure and assured that the K2 algorithm could reach the actual Asian network once the node sequence is given. The SHD indicator is used as a measure of the overall match between the predicted and standard structures. This indicator decreased with the increase in dataset number and gradually stabilized when the sample size reached the value of 2500. Thus, when the sample size reaches 2500, it is reasonable to construct the BN structural model using the MDK2-BN structure.

Table 1
BIC score under different amounts of data.

The number of samplesin the dataset	BIC score results			
	B_{best}	B_{wors}	B_{aver}	B_{stan}
500	-1219.8	-1236.6	-1228.4	-1215.1
1000	-2349.3	-2354.9	-2351.2	-2347.5
1500	-3627.1	-3644.2	-3630.9	-3625.7
2000	-4649.7	-4661.4	-4652.5	-4648.4
2500	-5218.3	-5233.8	-5221.3	-5217.8
3000	-6815.1	-6819.2	-6817.7	-6814.6
3500	-7936.7	-7941.7	-7939.6	-7936.5
4000	-9425.4	-9429.3	-9427.7	-9425.3

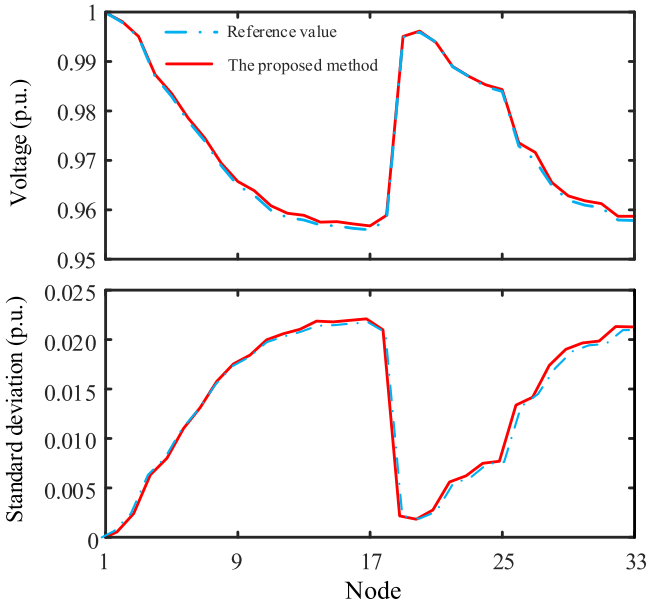

Fig. 5. Digital characteristics of nodal voltage amplitude.

The variation of BIC score at different data sizes is presented in Table 1, where B_{best}, B_{wors}, and B_{aver} denote the best, the worst, and the average BIC scores after 100 calculations, respectively; and B_{stan} represents the BIC score of the standard structure. As presented in Table 1, after the sample size reached the value of 2000, the optimal structure score B_{best} searched by our proposed method is almost the same as the score B_{stan} of the standard structure, which illustrates the effectiveness of proposed method in compressing the search space by constructing the largest support tree. When the sample size is less than 2000, there is a substantial difference between B_{wors} and B_{stan}. The main reason is that the small data size would reduce the accuracy of the maximum support tree orientation, but the joint DFS would gradually make up for the inaccuracy in the maximum support tree orientation. On the whole, a reasonably-accurate Bayesian network structure can be achieved for small networks when the node sequence is optimized by the MWST and DFS algorithms, followed by performing the K2 algorithm using the optimized node sequence as *a priori* knowledge.

6.2. *Verification of effectiveness of wind–photovoltaic–load joint scenarios*

IEEE 33-bus test system is selected for simulation analysis, and the voltage level is 12.66kV. DG includes WTG and PVG, and the historical data of wind speed, light intensity and load measured in this paper comes from Gansu Province, China, including the wind speed and light intensity samples collected by 6 observatories in the region in one year and the load data obtained simultaneously, a total of 8760 groups. WTG access buses 5, 9, and 15 with a rated power of 500KW, and PVG access

Table 2
Error of nodal voltage.

Method	Maximum deviation	Maximum relative deviation /%	Sum of deviations
500 scenes	3.428×10^{-3}	0.369	5.681×10^{-3}

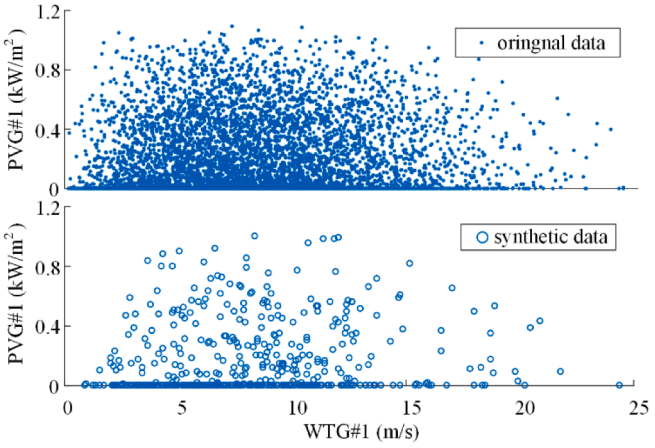

Fig. 6. Scattered plot of original data and synthetic data.

Table 3
IMPSO algorithm related parameters.

Population size	Iterative number	Update interval of ω_i	The acceleration coefficient C_1	C_2
100	200	[0.4,0.9]	2.5 decreased to 0.5	0.5 increasing to2.5

buses 3, 10, and 22 with a rated power of 500KW. The MDK2-BN model is used to generate 500 scenarios randomly, and then probabilistic power flow calculation is used to test whether the joint scenario can accurately and completely represent the nonlinear correlation of historical wind speed, light intensity and load demand. The results of deterministic load flow calculation based on the 8760 sets of wind-photovoltaic-load power data are the benchmark. The results of the combined calculation of wind–photovoltaic–load joint scenario are compared with the reference values. The digital characteristics of different nodal voltages are shown in Fig. 5, and the error of all nodal voltage are shown in Table 2.

The results in Fig. 5 and Table 2 show that the wind-photovoltaic-load joint scenario obtained by the MDK2-BN model is in good agreement with the calculated results of the original sample. The achieved calculation accuracy also verifies the effectiveness of the MDK2-BN model; namely, the sample obtained by the model maintain the basic probability characteristics of the original sample and the correlation between wind, photovoltaic, and load. In order to further investigate whether the synthetic data retains the non-linear related information of the original data, Fig. 6 shows the two-dimensional scatter plots of the original sample 8760 groups and the synthetic sample 500 groups. The shape of the scatter plot, the distribution of the data points, and the accumulation area are basically consistent with the original data.

6.3. Analysis of DG planning results

The relevant basic parameters are consistent with Section 6.2. It is planned to build three WTG and three PVG in six buses, and the candidate buses for WTG = [8 9 15 16 17 21 24 30 31 33], for PVG = [7 10 15 16 17 23 25 28 31 32]. The maximum allowable transmission

Table 4
Result analysis of the optimal planning results.

Project	Configuration result / MW (position) Scheme 1	Scheme 2	Scheme 3
WTG	0.74(15),0.76 (17),0.85(31)	0.67(9),0.59 (17),0.79(21)	0.45(8),0.37 (24),0.53(30)
PVG	0.57(10),0.73 (23),0.68(31)	0.51(17),0.64 (23),0.49(31)	0.32(7),0.46 (25),0.31(32)
C_I/(× 10^4 $)	12.61	10.87	7.21
C_{OM}/(× 10^4 $)	6.03	4.69	3.52
C_{IL}/(× 10^4 $)	3.81	4.97	5.32
C_P/(× 10^4 $)	129.35	170.83	154.86
I_S/(× 10^4 $)	140.61	117.78	78.02
I_G/(× 10^4 $)	6.67	5.24	3.45
I_R/(× 10^4 $)	97.52	82.17	53.74
I_E/(× 10^4 $)	6.19	—	3.76
f_2	0.0479	0.0616	0.0645

Table 5
Interruptible load point results.

Interruptible load position	Total annual interrupted power /(MW·h)
13	13.7
16	0
20	7.9
23	0
27	54.8

capacity of the line is set to 3.81MVA, the nodal voltage is restricted to 0.95~1.05p.u., and the load buses = [9 13 20 23 27] can be interrupted. The weight coefficients in Eq. (13) and Eq. (14) are both 0.5. The relevant settings of the IMPSO algorithm are shown in Table 3.

The proposed MDK2-BN model is used to generate 500 scenarios randomly, and then H-K composite clustering algorithm is used to compress them into 10 typical scenarios. Different planning schemes are set for analysis and comparison.

Scheme 1: Use the planning model proposed in this paper to obtain a DG configuration scheme that considers the indicators of the economy, system safety, and environmental benefit.

Scheme 2: Ignore the environmental benefits, and only consider the DG configuration solution for the economy and system safety. It is used to verify the effectiveness of the planning model considering environmental costs for optimizing access capacity.

Scheme 3: on the basis of the planning model in this paper, the location of DG grid connection is modified, according to the principle of high load level priority access, but the capacity of DG is limited within 80% of nodal load. It is used to verify the effectiveness of the proposed planning model for DG access location and capacity.

Table 4 shows that the configuration derived from Scheme 1 improved the grid access and absorption capability of the DG. Compared to Scheme 2 and Scheme 3, C_P in Scheme 1 decreased from 1.7083 million dollars and 1.5486 million dollars to 1.2935 million dollars, respectively, with the maximum reduction of 24.3%. Additionally, while lowering the grid configuration cost, Scheme 1 also reduced the grid operation risk by taking environmental benefits into account. Overall, although the DG access volume, investment, and operation costs are higher for Scheme 1 than the other schemes, Scheme 1 is more suitable in terms of economy, operation safety, and environmental benefits.

The interruption conditions of the load interruption points presented in Table 5 indicate that not all designated load interruption points are interrupted. For instance, bus-16 and bus-23 do not need to be

Table 6
DG optimization configuration.

Type of season	Maximum allowable capacity of DG / MW (corresponding position)		
	WTG	PVG	Total
Summer	0.52(9),0.43(15),0.64(25)	0.71(3),0.87(22),0.74(28)	3.91
Winter	0.77(16),0.82(21),0.93 (28)	0.53(17),0.58(22),0.49 (29)	4.12
Annual	0.74(15),0.76(17),0.85 (31)	0.57(10),0.73(23),0.68 (31)	4.33

interrupted because the voltages at these nodes are severely affected by the terminal node generator, and the demand for high load could be controlled directly by the generator. In contrast, when demand for high load occurred at bus-13, bus-20, and bus-27, which are located farther away from the end node, and when the DG output is low, the interruption is necessary to ensure stable system operation.

6.4. *Effects of seasonal fluctuation on DG configuration*

In order to demonstrate the effects of changes in the DG output and seasonal fluctuation of load demand on the DG configuration planning, the DG volume is considered as the only decision variable and the planning results for summer and winter seasons are compared with the planning results for the whole year. The planning results of the DG access capacity are shown in Table 6. The BN model for different DG variables is displayed in Fig. 7.

By comparing the BN model connection in different seasons shown in Fig. 7, it is found that PWG and PVG had strong autocorrelation behavior under all three conditions; this is represented by line connections between wind speed and wind speed and between light intensity and light intensity. In the summer, due to abundant light resources, PVG#1 has a direct effect on PWG#2, and load demand L#1 is also constrained by PVG#3. In the winter, when wind resources are more abundant, PWG#3 has a direct impact on PVG#1, while L1 shows a dependence relationship with PWG#2 and PVG#2. Over the whole year, the region is dominated by the wind speed performance, and the wind speed influence the light intensity of the line at the three nodes' locations. The regional wind–photovoltaic–load correlation characteristics are well preserved.

The results in Table 6 show that the maximum allowable capacity of PVG obtained in the summer is significantly higher than that of WTG, while the maximum allowable capacity of WTG obtained in the winter is significantly higher than that of PVG. This indicates that considering the complementary effects of the wind speed and light intensity on the output power is necessary for the capacity configuration. Therefore, the highest DG access capacity plan can be obtained by considering the spatiotemporal correlation of different seasons of the year. Hence, the waste of energy and material resources can be reduced, and energy utilization can be improved only when a policy conforms to the complementary nature of the actual DG output.

The Pareto leading edge driven by annual data and obtained by mainly considering the technology, economics, and environmental benefits is presented in Fig. 8. As shown in Fig. 8, there is an antagonistic relationship between the average annual profit rate of DG and the comprehensive operation risk. As the position and capacity of the DG changed, the results of both targets are impacted. The antagonistic nature of the two objectives makes it impossible to optimize both objective functions at the same time. The upward trends on the left- and right-hand sides of the marked point shows obvious differences. The average annual profit rate at the corresponding point is 1.93, and the system risk is 0.047.

The results presented in this section reveal that, based on the annual data, the installation capacity of WTG is generally higher than the installation capacity of PVG. This indicates that, when a certain number of wind turbine fields and photovoltaic solar energy fields are installed in a region at the same time, the wind turbine will have a higher priority. The reason is that wind resources are more abundant than solar resources. Increasing the wind power capacity can help to reduce the comprehensive annual cost for the investors and increase the revenue. As the annual average rate of return increases, the grid operation risk increases faster. Therefore, while focusing mainly on the high annual rate of return, the planners should also avoid instability in system security. A diverse feasible solution allows the planners to decide a suitable planning program from a dual perspective.

7. Conclusion

An innovative multi-objective DG planning model that

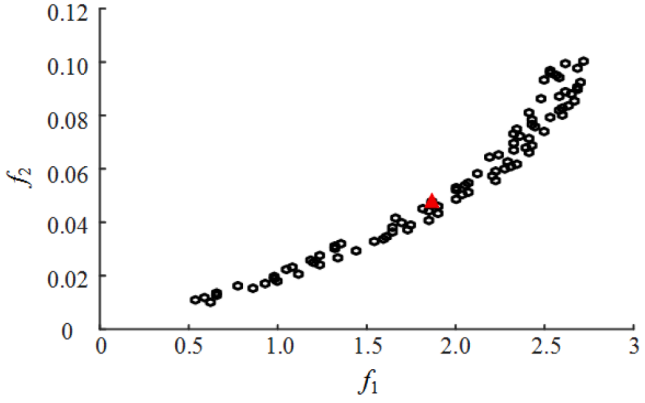

Fig. 8. Pareto optimal frontier

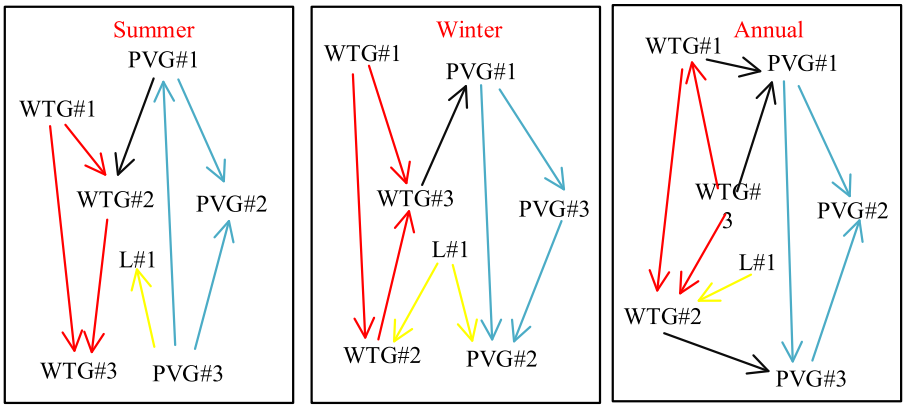

Fig. 7. BNs in different seasons.

comprehensively considers the economy, operational safety, and environmental benefits, is established. The seasonal changes in the correlation of photovoltaic and wind power generation show uncertain differences. Therefore, the simultaneous consideration of the seasonal changes and the spatiotemporal correlation characteristics between DG variables can not only increase the DG penetration rate, but also provide decision makers with a helpful reference for constructing the planning scheme from different perspectives. Further, it provides a MDK2-BN model to handle the spatiotemporal correlation between different types of DG and between DG and load. The achieved accuracy of flow calculations meets the engineering requirements. This paper provides useful ideas for DG planning driven by multi-dimensional wind–photovoltaic–load data and pertinent theoretical support for solving the planning problems with a strong spatiotemporal coupling of DG in adjacent regions.

CRediT authorship contribution statement

Fengyang Gao: Supervision, Writing – review & editing. **Cheng Yuan:** Conceptualization, Formal analysis, Writing – original draft, Software, Writing – review & editing. **Zhaojun Li:** Data curation, Formal analysis. **Shengxian Zhuang:** Investigation.

Declaration of Competing Interest

The authors declare that they do not have any known competing financial interests or personal relationships that could affect the work reported here.

Data availability

Data will be made available on request.

Acknowledgments

We gratefully acknowledge the support of the key Research and Development projects in gansu Province of China (NO. 18YF1FA058) and the talent innovation project in Lanzhou City of China (2017-RC-95).

References

[1] Z Abdmouleh, R A Alammari, A. Gastli, Review of policies encouraging renewable energy integration & best practices, Renew. Sustain. Energy Rev. 45 (2015) 249–262, https://doi.org/10.1016/j.rser.2015.01.035.
[2] M M Haque, P. Wolfs, A review of high PV penetrations in LV distribution networks: Present status, impacts and mitigation measures, Renew. Sustain. Energy Rev. 62 (2016) 1195–1208, https://doi.org/10.1016/j.rser.2016.04.025.
[3] S Zhang, H Cheng, K Li, et al., Optimal siting and sizing of intermittent distributed generators in distribution system, IEEJ Trans. Electr. Electron. Eng. 10 (6) (2015) 628–635, https://doi.org/10.1002/tee.22129.
[4] R H Zubo, G Mokryani, H-S Rajamani, et al., Operation and planning of distribution networks with integration of renewable distributed generators considering uncertainties: a review, Renew. Sustain. Energy Rev. 72 (2017) 1177–1198, https://doi.org/10.1016/j.rser.2016.10.036.
[5] H Jia, W Qi, Z Liu, et al., Hierarchical risk assessment of transmission system considering the influence of active distribution network, IEEE Trans. Power Syst. 30 (2) (2014) 1084–1093, https://doi.org/10.1109/tpwrs.2014.2360851.
[6] D Schindler, H D Behr, C. Jung, On the spatiotemporal variability and potential of complementarity of wind and solar resources, Energy Convers. Manag. 218 (2020), 113016, https://doi.org/10.1016/j.enconman.2020.113016.
[7] Y Liu, H Qin, Z Zhang, et al., Probabilistic spatiotemporal wind speed forecasting based on a variational Bayesian deep learning model, Appl. Energy 260 (2020), 114259, https://doi.org/10.1016/j.apenergy.2019.114259.
[8] A Jarraya, P Leray, A. Masmoudi, Discrete exponential Bayesian networks: definition, learning and application for density estimation, Neurocomputing 137 (2014) 142–149, https://doi.org/10.1016/j.neucom.2013.05.061.
[9] B Moradabadi, H. Beigy, A new real-coded Bayesian optimization algorithm based on a team of learning automata for continuous optimization, Genet. Program. Evolv. Mach. 15 (2) (2014) 169–193, https://doi.org/10.1007/s10710-013-9206-9.
[10] H Wang, B. Zou, Probabilistic computational model for correlated wind speed, solar irradiation, and load using Bayesian network, IEEE Access 8 (2020) 51653–51663, https://doi.org/10.1109/ACCESS.2020.2977727.
[11] X YANG, M MAIHEMUTI, S LIU, State assessment method of capacity reduction at high temperature for wind turbine based on vine-copula Bayesian network model, in: Proceedings of the CSEE, 2020, https://doi.org/10.13334/j.0258-8013.pcsee.191157.
[12] E Perrier, S Imoto, S. Miyano, Finding optimal Bayesian network given a super-structure, J. Mach. Learn. Res. 9 (10) (2008), https://doi.org/10.1007/s10883-008-9053-9.
[13] I Tsamardinos, LE Brown, CF Aliferis, The max-min hill-climbing Bayesian network structure learning algorithm, Machine Learn. 65 (1) (2006) 31–78, https://doi.org/10.1007/s10994-006-6889-7.
[14] M Gasse, A Aussem, H Elghazel, A hybrid algorithm for Bayesian network structure learning with application to multi-label learning, Expert Syst. Appl. 41 (15) (2014) 6755–6772, https://doi.org/10.1016/j.eswa.2014.04.032.
[15] J A Gámez, J L Mateo, J M Puerta, Learning Bayesian networks by hill climbing: efficient methods based on progressive restriction of the neighborhood, Data Min. Knowl. Discov. 22 (1) (2011) 106–148, https://doi.org/10.1007/s10618-010-0178-6.
[16] S Zhang, H Cheng, K Li, et al., Multi-objective distributed generation planning in distribution network considering correlations among uncertainties, Appl. Energy 226 (2018) 743–755, https://doi.org/10.1016/j.apenergy.2018.06.049.
[17] K Li, N TAI, S ZHANG, Multi-objective planning method of distributied generators considering correlations, Automation of Electr. Power Syst. 41 (9) (2017) 51–57, https://doi.org/10.7500/AEPS20160805001. + 199. (in Chinese).
[18] M SUN, Parallel optimal allocation of distributed PV in distribution network considering active management, Electr. Power Autom. Equip. 39 (3) (2019) 169–174, https://doi.org/10.16081/j.issn.1006-6047.2019.03.027. + 181. (in Chinese).
[19] S ZHANG, Siting and sizing planning of distributed wind generators under active management mode, Automation of Electr. Power Syst. 39 (9) (2015) 208–214, https://doi.org/10.7500/AEPS20140409015 (in Chinese).
[20] B CHEN, Capacity planning strategies for distributed generation considering wind-photovoltaic-load joint time sequential scenarios, Power Syst. Technol. 42 (3) (2018) 755–761, https://doi.org/10.13335/j.1000-3673.pst.2017.1304, in Chinese.
[21] J M Home-Ortiz, M Pourakbari-Kasmaei, M Lehtonen, et al., Optimal location-allocation of storage devices and renewable-based DG in distribution systems, Electr. Power Syst. Res. 172 (2019) 11–21, https://doi.org/10.1016/j.epsr.2019.02.013.
[22] O Penangsang, D F U Putra, T. Kurniawan, Optimal placement and sizing of distributed generation in radial distribution system using K-means clustering method, in: 2017 International Seminar on Intelligent Technology and Its Applications (ISITIA); 2017, IEEE, 2017, pp. 98–103, https://doi.org/10.1109/ISITIA.2017.8124062.
[23] H Sun, J Liu, C. Peng, Multi-objective DG planning based on classified probability integration multi-scenario analysis, Electr. Power Autom. Equip. 38 (12) (2018) 45–51, https://doi.org/10.16081/j.issn.1006-6047.2018.12.006, in Chinese.
[24] V Thapar, G Agnihotri, V K Sethi, Critical analysis of methods for mathematical modelling of wind turbines, Renew. Energy 36 (11) (2011) 3166–3177, https://doi.org/10.1016/j.renene.2011.03.016.
[25] J I Alonso, L de la Ossa, J A Gamez, et al., On the use of local search heuristics to improve GES-based Bayesian network learning, Appl. Soft Comp. 64 (2018) 366–376, https://doi.org/10.1016/j.asoc.2017.12.011.
[26] M Scanagatta, G Corani, C P De Campos, et al., Approximate structure learning for large Bayesian networks, Mach. Learn. 107 (8) (2018) 1209–1227, https://doi.org/10.1007/s10994-018-5701-9.
[27] P Ratnapinda, MJ Druzdzel, Learning discrete Bayesian network parameters from continuous data streams: What is the best strategy? J. Appl. Logic 13 (4) (2015) 628–642, https://doi.org/10.1016/j.jal.2015.03.007.
[28] S Behjati, H. Beigy, Improved K2 algorithm for Bayesian network structure learning, Eng. Appl. Artif. Intell. 91 (2020), 103617, https://doi.org/10.1016/j.engappai.2020.103617.
[29] F Wang, Y Zhuang, H Gu, et al., Octreenet: a novel sparse 3-d convolutional neural network for real-time 3-d outdoor scene analysis, IEEE Trans. Autom. Sci. Eng. 17 (2) (2019) 735–747, https://doi.org/10.1109/TASE.2019.2942068.
[30] R A Fisher, On the mathematical foundations of theoretical statistics, Philos. Trans. R. Soc. Lond. Ser. 222 (594–604) (1922) 309–368, https://doi.org/10.2307/91208. A Containing Papers of a Mathematical or Physical Character.
[31] Y Jingxu, Y Yingqi, Z. Yonglun, Operation risk analysis of electric vehicle integrated to grid in distribution network based on weighted distribution entropy, Autom. Electr. Power Syst. 44 (05) (2020) 171–179, https://doi.org/10.7500/AEPS20190303007.
[32] W Hu, G G Yen, Adaptive multiobjective particle swarm optimization based on parallel cell coordinate system, IEEE Trans. Evolut. Comp. 19 (1) (2013) 1–18, https://doi.org/10.1109/TEVC.2013.2296151.
[33] C Yue, B Qu, J. Liang, A multiobjective particle swarm optimizer using ring topology for solving multimodal multiobjective problems, IEEE Trans. Evolut. Comp. 22 (5) (2017) 805–817, https://doi.org/10.1109/TEVC.2017.2754271.
[34] M Hu, T Wu, J D Weir, An adaptive particle swarm optimization with multiple adaptive methods, IEEE Trans. Evolut. Comp. 17 (5) (2012) 705–720, https://doi.org/10.1109/TEVC.2012.2232931.
[35] S Ding, C Chen, B Xin, et al., A bi-objective load balancing model in a distributed simulation system using NSGA-II and MOPSO approaches, Appl. Soft Comp. 63 (2018) 249–267, https://doi.org/10.1016/j.asoc.2017.09.012.